Locally disrupted synchronization in Langevin molecular dynamics

Andreea I. Georgescu, Samuel J. Denny, Emilien Joly, Grace Chen, Danny Perez, and Arthur F. Voter

Phys. Rev. E **86**, 026703 — Published 3 August 2012

DOI: 10.1103/PhysRevE.86.026703

Locally Disrupted Synchronization in Langevin Molecular Dynamics

Andreea I. Georgescu,[1] Samuel J. Denny,[2] Emilien Joly,[3] Grace Chen,[4] Danny Perez,[5] and Arthur F. Voter[5,*]

[1] *Physics and Astronomy, University of California Los Angeles, 430 Portola Pl, Los Angeles, California 90095, USA*
[2] *Clarendon Laboratory, University of Oxford, Parks Road, Oxford, OX1 3PU, UK*
[3] *ENS Cachan, 61 avenue du Président Wilson 94235 Cachan, France*
[4] *Gould School of Law, University of Southern California, 699 Exposition Boulevard, Los Angeles, California 90089, USA*
[5] *Theoretical Division, Los Alamos National Laboratory, Los Alamos, New Mexico 87545, USA*

Stochastic thermostats commonly used in molecular dynamics trajectories are known, under certain conditions, to exhibit a synchronization effect whereby trajectories initialized at different points in phase space synchronize to a single master trajectory if they are subjected to the same sequence of random forces. We investigate the spatio-temporal robustness of this effect analytically and with molecular dynamics simulations in one and three dimensions in the strong coupling limit. We first investigate the response of the system to a time- and space-wise local perturbation and show that desynchronization behaves diffusively at long times for infinite systems. We then explore the behavior of temporally persistent but spatially local perturbations and observe strikingly different behaviors as a function of dimensionality: in one dimension, the desynchronization propagates through the whole lattice and grows with time, while in three dimensions, the desynchronization remains localized in the neighborhood of the perturbation.

PACS numbers: 05.10.Gg,05.45.Xt,83.10.Rs,33.15.Vb

I. INTRODUCTION

Molecular dynamics (MD) simulations — the numerical integration of atomistic equations of motion — find applications across a broad range of disciplines, allowing for atomic-scale studies within chemistry, materials science and biology.

In many cases, it is desirable to advance the equations of motion in a way that is appropriate for a thermal system, i.e., to mimic canonical ensemble behavior (characterized by fixed temperature, volume, and particle number). Two widely used methods that successfully achieve canonical sampling are the Andersen [1] and the Langevin [2] thermostats. Both of these are stochastic in nature, as they use pseudo-random numbers in the equations of motion to introduce noise into the systems, which mimic random solvent collisions. Previous studies have revealed that stochastic thermostats have a rather interesting property: under suitable conditions, two thermostatted trajectories subject to identical stochastic force sequences, but having different initial conditions, can synchronize in phase space to a single "master trajectory". The phenomenon has been observed for a wide range of potentials and temperatures, and even for rather complex systems. Fahy and Hamman [3] found the rate of synchronization for regular-time Andersen thermostat, while Maritan and Banavar [4], and Ciesla et al. [5] observed synchronization in Langevin thermostats. Uberuaga et al. [6] studied the synchronization dynamics as a function of the thermostat coupling strength for harmonic potentials. They also demonstrated that synchronization occurs for a system of 97 atoms interacting via a many-body interatomic potential. Finally, Sindhikara and co-workers showed the effect occurs even for complex biological molecules [7].

In this paper, we further characterize the evolution of this synchronization effect through space and time. We focus on the Langevin thermostat, for which the classical equations of motion are augmented by viscous drag and Gaussian-distributed stochastic forces. By deriving equations of motions for the desynchronization in the continuum limit, we first analyze the response of one- and three-dimensional systems to an instantaneous perturbation (localized in time and space, such as poking one atom at $t = 0$). We show that the propagation of the desynchronization becomes diffusive at large times. We validate the results against one- and three-dimensional face-centered cubic (FCC) crystals interacting via the Lennard-Jones potential in the high friction limit. However, we emphasize that the results are not confined to a particular type of potential or crystal structure.

Building on the results for an instantaneous perturbation, we extend the analysis to treat time-persistent perturbations, such as changing the sequence of random forces on one single atom (while leaving all other forces the same). In doing so, we discover an interesting effect. Due to the persistent randomness induced by the stochastic forces, one might expect that the distance in phase-space between the two simulations would increase and the simulations would become statistically independent. This intuition is confirmed for infinite one-dimensional systems, where the root mean square (rms) of the desynchronization (taken over many simulations with different

*afv@lanl.gov

random seeds) continuously grows with time for every atom in the chain. However, for three-dimensional crystals the behavior is found to be quite different. We find that for every atom in the crystal, instead of growing to infinity, the rms desynchronization reaches a constant asymptotic value. Furthermore, the desynchronization remains localized around the center of disturbance, and falls with distance roughly as $1/r^2$ at long times.

Our results demonstrate the robustness of the Langevin synchronization effect; for a three-dimensional system, even a persistent, random force applied to this atom only disrupts the synchronization locally, while distant parts of the system remain well synchronized. Aside from our interest in this Langevin synchronization phenomenon at a fundamental level, exploring the characteristics of this synchronization increases our understanding of modern atomistic simulation methods that employ stochastic thermostats, which is helpful both for avoiding the potential pitfalls [7] as well as in the development of new methods. For example, a parallel-in-time algorithm for accelerating infrequent events can be formulated by exploiting synchronization [6]. The understanding developed here, that a transient force error in a three-dimensional system is self-correcting, and even a persistent force error of the right nature only modifies the dynamics in a spatially local way, should be useful in this regard. This behavior could be exploited for example on a computer architecture for which there may be occasional, brief errors in the atomic forces. While for many algorithms this could not be tolerated, a molecular dynamics simulation coupled to a Langevin thermostat would maintain high accuracy in the face of this.

The paper is organized as follows: in Section II, we derive analytical expressions for the response of one- and three-dimensional systems to perturbations that are local in space and time. These results are validated through comparison with MD simulations in Section III. Our analysis is extended to temporally persistent perturbations in Section IV, and these results are also validated through comparison with direct MD simulations in Section V.

II. INSTANTANEOUS PERTURBATIONS: "POKING"

As discussed above, we are interested in characterizing the evolution of the desynchronization in Langevin dynamics caused by an external perturbation. In this section we consider an instantaneous and spatially localized disturbance: a single poke of a single atom in the lattice. Between two otherwise identical simulations, we consider the differences resulting from the addition of an initial velocity V to a single atom.

We begin developing the theory by obtaining the equation of motion that describes the evolution of the disturbance in space and time. We consider either one or three-dimensional lattices of atoms of mass m. Throughout the paper we define a to be the equilibrium distance between the nearest-neighbor atoms. Denoting the position of the i^{th} atom with x_i and the net force acting upon it with $F_i = -\partial U/\partial x_i$, with U to total potential energy of the system, the equations of motion under Langevin dynamics read:

$$\ddot{x}_i + \alpha \dot{x}_i = \frac{1}{m} F_i + \frac{1}{m} A_i. \tag{1}$$

$A_i(t)$ is a function of time and represents the stochastic force acting on atom i. Setting the noise sequence $A_i\,(t)$ of any atom i to be identical for both runs, the desynchronization $u_i(t) = x_i^{(2)}(t) - x_i^{(1)}(t)$ resulting from the poke evolves according to:

$$\ddot{u}_i + \alpha \dot{u}_i = \frac{1}{m} \Delta F_i, \tag{2}$$

where $\Delta F_i(t) = F_i^{(2)}(t) - F_i^{(1)}(t)$ is the difference in forces acting on atom i between the two runs. At low enough temperature, the potential energy of the system can be considered quadratic in the displacement from equilibrium, i.e., $U \simeq (x - x_{eq})^T H (x - x_{eq})$ where H is the Hessian matrix defined as $H_{ij} = \partial^2 U/\partial x_i \partial x_j$. The equation of motion of the desynchronization then becomes:

$$\ddot{u} + \alpha \dot{u} = -\frac{1}{m} H u. \tag{3}$$

A. Infinite one-dimensional harmonic chain

We start with the evolution of the desynchronization in the continuum limit in one dimension, and we will later investigate three-dimensional lattices. In one dimension, the right-hand-side of Eq (3) directly corresponds to a discretized form of the second derivative of the desynchronization (this can also be obtained in the general case through a small wavevector expansion), and the discrete equation of motion can be written as a damped wave equation:

$$\frac{\partial^2 u}{\partial t^2} + \alpha \frac{\partial u}{\partial t} - c^2 \frac{\partial^2 u}{\partial x^2} = 0, \tag{4}$$

where c is the propagation speed of the wave through the medium. Applying a poke of strength V at $(x,t) = (0,0)$ and accounting for the fact that in one dimension there is one atom per length a, the initial conditions are:

$$u(x,0) = 0 \tag{5}$$

$$\frac{\partial u}{\partial t}(x,0) = V \delta\left(\frac{x}{a}\right), \tag{6}$$

where δ is the Dirac-delta function. Using Riemann's Method [8] to solve this equation, we obtain:

$$u(x,t) = \begin{cases} \frac{aV}{2c} e^{-\frac{1}{2}\alpha t} I_0\left(\frac{\alpha}{2c}\sqrt{(ct)^2 - x^2}\right), & |x| < ct \\ 0, \text{ otherwise,} \end{cases} \tag{7}$$

where $I_0(\xi)$ is a modified Bessel function of the first kind and order 0. This solution is restricted to the overdamped case, as we will see later in Section II B. This central result for the one-dimensional chain is compared with a molecular dynamics simulation of a Lennard-Jones chain in Section III A.

It is insightful to consider the large time limit of the above result, making use of the asymptotic form of I_n for large arguments [9], namely

$$I_n(\xi) \to \frac{e^{\xi}}{\sqrt{2\pi\xi}} \quad \text{for } \xi \gg 1, \tag{8}$$

which yields:

$$u(x,t) \to \frac{aV}{c\sqrt{4\pi\alpha t}} e^{-\frac{\alpha x^2}{4c^2 t}} \quad \text{for } t \gg \frac{1}{\alpha},\ |x| \ll ct. \tag{9}$$

Although $|x| \ll ct$ is formally required, at large time the desynchronization around $x \approx ct$ is very close to zero and the discontinuity at $x = ct$ becomes unobservable. Therefore, only the requirement $t \gg \frac{1}{\alpha}$ remains of practical importance and Eq (9) can be taken as approximately valid for all x.

Eq (9) implies that at large time the desynchronization is the fundamental solution to the diffusion equation:

$$\alpha \frac{\partial u}{\partial t} = c^2 \frac{\partial^2 u}{\partial x^2} \tag{10}$$

for initial conditions:

$$u(x,0) = \frac{V}{\alpha}\delta\left(\frac{x}{a}\right) \tag{11}$$

$$\frac{\partial u}{\partial t}(x,0) = 0. \tag{12}$$

This implies that the total integrated desynchronization is conserved during further evolution.

B. Periodic one-dimensional harmonic chain

Consider now a finite lattice of length L with periodic boundary conditions, where again we poke the atom located at $x = 0$ at time $t = 0$. This can also be treated as an infinite lattice with periodic pokes, i.e. we can solve Eq (4) with initial conditions:

$$u(x,0) = 0 \tag{13}$$

$$\dot{u}(x,0) = V \sum_{n\in\mathbb{Z}} \delta\left(\frac{x - nL}{a}\right), \tag{14}$$

where L is the lattice size. The solution for a finite periodic lattice is then a superposition of the solutions for one poke, and we find:

$$u_{\text{pbc}}(x,t) = \sum_{n\in\mathbb{Z}} u(nL + x, t). \tag{15}$$

Here u is given by Eq (7), or Eq (9) at large times. As shown in the previous section in Eq (7), all atoms with $|x| > ct$ are completely synchronized. Therefore, the solution for a finite lattice with periodic boundary conditions remains identical within one period to the solution for an infinite lattice until the desynchronization wave reaches the boundaries of the lattice (thus until $ct = L/2$).

Since our lattice is now finite, another effect needs to be considered. Adding a poking velocity V to one of the atoms induces an initial drift velocity V/N of the entire lattice where N is the number of atoms. Due to damping, the two systems will continue to desynchronize with drift velocity $v_{\text{drift}}(t) = V/N e^{-\alpha t}$, which results in a shift of the center of mass of the lattice equal to $V/(\alpha N)(1 - e^{-\alpha t})$. In order to correct for this, we subtract the displacement of the center of mass from the position of each atom. The resulting desynchronization for periodic boundary conditions after subtracting the displacement of the center of mass becomes:

$$u_{\text{pbc}}(x,t) = \sum_{n\in\mathbb{Z}} u(nL + x, t) - \frac{1}{L}\int_{-\infty}^{\infty} u(x', t)\, dx'. \tag{16}$$

In the second term on the right hand side of the equation we have exploited the fact that integrating the desynchronization from a single poke over an infinite space is equivalent to summing the contributions from the infinite set of pokes and integrating that over one period. Using the large time limit as in Eq (9) and rewriting Eq (16) in terms of its Fourier series, we obtain the following for the desynchronization:

$$u_{\text{pbc}}(x,t) = \frac{2aV}{\alpha L} \sum_{n\geq 1} e^{-\frac{\omega_0^2 n^2}{\alpha} t} \cos(n k_0 x) \tag{17}$$

where $\omega_0 = 2\pi c/L = c\, k_0$ is the fundamental frequency.

The solution represents the exponential decay of the normal modes amplitude in a one-dimensional lattice at high friction. The desynchronization was obtained by taking the sum over all modes with $n > 0$ of the Fourier transform of Eq (9). The mode with $n = 0$ corresponded to the drift of the center of mass of the lattice, which was excluded from the result. The cosine factor gives the desynchronization of the other atoms in the lattice as a function of distance from the poked atom.

For each mode, the decay matches the result obtained by Uberuaga et al. [6, Eqs 5-7] in the limit of high friction (for the overdamped case). If one was to consider oscillations in a harmonic potential (as in Eq (4)), the full solution for each mode would be

$$u_n(x,t) = \frac{2aV}{\alpha L} e^{-\alpha t/2} \text{Re}\left(e^{\sqrt{\alpha^2 - 4n^2\omega_0^2}\,\frac{t}{2}}\right) \cos(n k_0 x), \tag{18}$$

which is overdamped for $\alpha > 2n\omega_0$, and underdamped otherwise.

As we will see in Section III when we compare to MD simulations, it is enough to require that α is sufficiently

large to make the lowest few modes overdamped. As long as the contribution from the high-frequency underdamped modes is small even at low time compared to the analytical prediction from Eq (7), then these modes act as high-frequency small oscillations superimposed on the analytical results from Eqs (4) and (8) (for the infinite chain), or (17) (for periodic boundary conditions).

At long times, the higher frequency modes decay at a higher rate, and the solution for periodic boundary conditions reduces only to the dominant term:

$$u_{\mathrm{pbc}}(x,t) \approx \frac{2aV}{\alpha L} e^{-\frac{\omega_0^2}{\alpha}t} \cos(kx) \qquad \text{for } t \gg \frac{\alpha}{4\omega_0^2}, \quad (19)$$

which, in contrast to the infinite lattice, corresponds to an exponential decay of the desynchronization with time.

C. Three dimensional lattice

A similar treatment is possible for three-dimensional perfect crystals. Starting from Eq (3) and carrying out a low wavevector expansion, one can obtain a general continuum wave equation of the form [10]:

$$\ddot{\boldsymbol{u}}_i + \alpha \dot{\boldsymbol{u}} = \frac{1}{\rho} \sum_{j,k,l} c_{i,j,k,l} \frac{\partial^2 \boldsymbol{u}_k}{\partial x_j \partial x_l}, \quad (20)$$

where $c_{i,j,k,l}$ are the elastic constants of the solid and ρ is its density. For elastically isotropic solids, this equation takes the simpler form:

$$\begin{aligned} \ddot{\boldsymbol{u}} + \alpha \dot{\boldsymbol{u}} &= \frac{1}{\rho}\left((\lambda+\mu)\nabla(\nabla\cdot\boldsymbol{u}) + \mu\nabla^2\boldsymbol{u}\right) \\ &= \frac{1}{\rho}\left((\lambda+2\mu)\nabla(\nabla\cdot\boldsymbol{u}) - \mu\nabla\times(\nabla\times\boldsymbol{u})\right). \end{aligned} \quad (21)$$

Here λ and μ are the Lamé parameters describing the elastic properties of the medium [11]. The longitudinal and transverse propagation speeds of the wave through the lattice are respectively:

$$c_l^2 = \frac{\lambda+2\mu}{\rho}, \qquad c_t^2 = \frac{\mu}{\rho}. \quad (22)$$

For poking of an atom in the z-direction, the initial conditions imposed on the system in three dimensions are:

$$\begin{aligned} \boldsymbol{u}(\boldsymbol{r},0) &= 0 \\ \dot{\boldsymbol{u}}(\boldsymbol{r},0) &= V\delta\left(\frac{\boldsymbol{r}}{l}\right)\hat{\boldsymbol{z}} \end{aligned} \quad (23)$$

where $\hat{\boldsymbol{z}}$ is the unit vector in z direction and l is a length element such that there is one atom per volume of l^3. For a face-centered cubic lattice (as investigated in the next section) there are four atoms per unit cell with volume of $\left(\sqrt{2}a\right)^3$, or equivalently one atom per volume of $l^3 = a^3/\sqrt{2}$.

Since the desynchronization field and its partial derivatives are continuous, we can write $\boldsymbol{u}(\boldsymbol{r},t)$ as the sum of an irrotational (curl-free) vector field and a solenoidal (divergence-free) vector field according to Helmholtz's theorem [12]:

$$\boldsymbol{u}(\boldsymbol{r},t) = \boldsymbol{f}(\boldsymbol{r},t) + \boldsymbol{h}(\boldsymbol{r},t) \quad (24)$$

$$\begin{aligned} \boldsymbol{f}(\boldsymbol{r},t) &= -\nabla\psi(\boldsymbol{r},t) \quad \text{s.t.} \quad \nabla\times\boldsymbol{f} = 0 \\ \boldsymbol{h}(\boldsymbol{r},t) &= \nabla\times\boldsymbol{A}(\boldsymbol{r},t) \quad \text{s.t.} \quad \nabla\cdot\boldsymbol{h} = 0. \end{aligned} \quad (25)$$

Given that differentiation with respect to time commutes with differentiation with respect to the spatial coordinates, we obtain that the irrotational and solenoidal parts of the time derivative $\dot{\boldsymbol{u}}$ are the same as the time derivatives of $\boldsymbol{f}$ and $\boldsymbol{h}$ respectively:

$$\mathrm{irrot}(\dot{\boldsymbol{u}}) = \dot{\boldsymbol{f}} \quad \text{and} \quad \mathrm{solen}(\dot{\boldsymbol{u}}) = \dot{\boldsymbol{h}}. \quad (26)$$

Consequently, Eq (21) decouples into two separate equations:

$$\begin{aligned} \ddot{\boldsymbol{f}} + \alpha\dot{\boldsymbol{f}} &= c_l^2\nabla(\nabla\cdot\boldsymbol{f}) \\ \ddot{\boldsymbol{h}} + \alpha\dot{\boldsymbol{h}} &= -c_t^2\nabla\times\nabla\times\boldsymbol{h}. \end{aligned} \quad (27)$$

Consider first the particular case of equal longitudinal and transverse propagation speeds $c \equiv c_l = c_t$ in Eq (21). In this case, the desynchronization obeys the following damped wave equation

$$\ddot{\boldsymbol{u}} + \alpha\dot{\boldsymbol{u}} = c^2\nabla^2\boldsymbol{u} \quad (28)$$

with solution $\boldsymbol{u}(\boldsymbol{r},t) = u(r,t)\hat{\boldsymbol{z}}$, for:

$$u(r,t) = \begin{cases} \dfrac{l^3V\alpha}{8c^2\pi\sqrt{(ct)^2-r^2}} e^{-\frac{1}{2}\alpha t} I_1\left(\frac{\alpha}{2c}\sqrt{(ct)^2-r^2}\right), \\ \qquad r < ct \\ \\ 0, \ \text{otherwise.} \end{cases} \quad (29)$$

In the equation above, I_1 is the modified Bessel function of the first kind and order one. Similarly to the one-dimensional case, we use the large argument limit of the Bessel function from Eq (8) to find the desynchronization at large times: $\boldsymbol{u}(\boldsymbol{r},t) = g(r,t)\hat{\boldsymbol{z}}$, where $g(r,t)$ is the three-dimensional Gaussian:

$$g(r,t) = \frac{l^3V}{c^3}\frac{\sqrt{\alpha}}{(4\pi t)^{3/2}} e^{-\frac{\alpha r^2}{4c^2 t}} = \frac{l^3V}{\alpha}\frac{1}{(\sqrt{2\pi}\sigma)^3} e^{-\frac{r^2}{2\sigma^2}}. \quad (30)$$

Here σ denotes the standard deviation of the Gaussian distribution above, and is given by:

$$\sigma(t) = \sqrt{\frac{2t}{\alpha}}c. \quad (31)$$

Note that the three-dimensional Gaussian is the fundamental solution to the diffusion equation $\alpha\dot{g}(r,t) = c^2\nabla^2 g(r,t)$.

From all of the above, and by analogy to the overdamped one-dimensional chain, we expect that for times below a few multiples of $1/\alpha$ a sharp front of desynchronization will propagate outwards from the poke, while at longer times, the desynchronization propagation will become diffusive. As a result, even for different propagation speeds c_l and c_t, at large times we expect that the desynchronization obeys the elastic diffusion equation

$$\alpha \dot{\boldsymbol{u}} = c_l^2 \nabla (\nabla \cdot \boldsymbol{u}) - c_t^2 \nabla \times \nabla \times \boldsymbol{u} \tag{32}$$

with boundary conditions:

$$\begin{aligned} \boldsymbol{u}(\boldsymbol{r}, 0) &= \frac{V}{\alpha} \delta\left(\frac{\boldsymbol{r}}{l}\right) \hat{\boldsymbol{z}} \\ \dot{\boldsymbol{u}}(\boldsymbol{r}, 0) &= 0. \end{aligned} \tag{33}$$

For simplicity, from this point on we will only be concerned with the elastic diffusion equation above, and we proceed to solve it for arbitrary longitudinal and transverse speeds.

As $g(r,t)$ is smooth and decays exponentially at infinity, we can decompose $\boldsymbol{u} = g\hat{\boldsymbol{z}}$ into its irrotational and solenoidal parts according to Helmholtz's theorem. The derivation is presented in the Appendix. Generalizing for a poke in an arbitrary direction $\hat{\boldsymbol{n}}$, the solution for the irrotational part is:

$$\begin{aligned} \boldsymbol{f}(\boldsymbol{r}, t) = &- \hat{\boldsymbol{r}}(\hat{\boldsymbol{n}} \cdot \hat{\boldsymbol{r}}) f_r(r,t) \\ &- \hat{\boldsymbol{\theta}}(\hat{\boldsymbol{n}} \cdot \hat{\boldsymbol{\theta}}) f_\theta(r,t) - \hat{\boldsymbol{\phi}}(\hat{\boldsymbol{n}} \cdot \hat{\boldsymbol{\phi}}) f_\phi(r,t). \end{aligned} \tag{34}$$

This generalization will be needed later in Section IV, when we will use these solutions to describe temporally persistent perturbations. The solenoidal part is then easily obtained from

$$\boldsymbol{h} = \hat{\boldsymbol{n}} g(r,t) - \boldsymbol{f} \tag{35}$$

and has the same angular dependence as $\boldsymbol{f}$.

Simplifying the above equations for a poke in $\hat{\boldsymbol{z}}$, we obtain for $\boldsymbol{f}$ and $\boldsymbol{g}$:

$$\boldsymbol{f}(r,\theta,t) = \hat{\boldsymbol{r}} \cos(\theta) f_r(r,t) + \hat{\boldsymbol{\theta}} \sin(\theta) f_\theta(r,t) \tag{36}$$

$$\boldsymbol{h}(r,\theta,t) = \hat{\boldsymbol{r}} \cos(\theta) h_r(r,t) + \hat{\boldsymbol{\theta}} \sin(\theta) h_\theta(r,t). \tag{37}$$

The ϕ components are zero (as expected from rotational symmetry around the z-axis), while the dependence on the angle θ of the r and θ components separates from r and t as shown above.

We find:

$$\begin{aligned} f_r(r,t) = &\frac{l^3 V}{\alpha} \frac{1}{(2\pi\sigma^2)^{3/2}} \\ &\left(e^{-\frac{r^2}{2\sigma^2}} \left(1 + \frac{2\sigma^2}{r^2}\right) - \sqrt{\pi} \frac{(\sqrt{2}\sigma)^3}{r^3} \mathrm{erf}\left(\frac{r}{\sqrt{2}\sigma}\right) \right) \end{aligned} \tag{38}$$

$$\begin{aligned} f_\theta(r,t) = f_\phi(r,t) = &\frac{l^3 V}{\alpha} \frac{1}{(2\pi\sigma^2)^{3/2}} \\ &\frac{1}{2} \left(e^{-\frac{r^2}{2\sigma^2}} \frac{2\sigma^2}{r^2} - \sqrt{\pi} \frac{(\sqrt{2}\sigma)^3}{r^3} \mathrm{erf}\left(\frac{r}{\sqrt{2}\sigma}\right) \right) \end{aligned} \tag{39}$$

$$\begin{aligned} h_r(r,t) = &-\frac{l^3 V}{\alpha} \frac{1}{(2\pi\sigma^2)^{3/2}} \\ &\left(e^{-\frac{r^2}{2\sigma^2}} \frac{2\sigma^2}{r^2} - \sqrt{\pi} \frac{(\sqrt{2}\sigma)^3}{r^3} \mathrm{erf}\left(\frac{r}{\sqrt{2}\sigma}\right) \right) \end{aligned} \tag{40}$$

$$\begin{aligned} h_\theta(r,t) = h_\theta(r,t) = &-\frac{l^3 V}{\alpha} \frac{1}{(2\pi\sigma^2)^{3/2}} \\ &\frac{1}{2} \left(e^{-\frac{r^2}{2\sigma^2}} \left(2 + \frac{2\sigma^2}{r^2}\right) - \sqrt{\pi} \frac{(\sqrt{2}\sigma)^3}{r^3} \mathrm{erf}\left(\frac{r}{\sqrt{2}\sigma}\right) \right). \end{aligned} \tag{41}$$

In the above $\sigma(t)$ is given in Eq (31).

We can rewrite Eqs (38)-(41) using the fact that the erf function can be written in terms of the confluent hypergeometric function of the first kind ${}_1F_1(a;b;z)$ (sometimes also denoted as $M(a,b,z)$) [13]:

$$\mathrm{erf}(z) = \frac{2z}{\sqrt{\pi}} e^{-z^2} {}_1F_1\left(1; \frac{3}{2}; z^2\right). \tag{42}$$

This yields:

$$f_r(r,t) = (1 + P(r,t))\, g(r,t) \tag{43}$$

$$f_\theta(r,t) = \frac{P(r,t)}{2} g(r,t) \tag{44}$$

$$h_r(r,t) = -P(r,t) g(r,t) \tag{45}$$

$$h_\theta(r,t) = -\left(1 + \frac{P(r,t)}{2}\right) g(r,t) \tag{46}$$

where we have defined

$$P(r,t) = \frac{2\sigma^2}{r^2} \left(1 - 2\, {}_1F_1\left(1; \frac{3}{2}; \frac{r^2}{2\sigma(t)^2}\right)\right), \tag{47}$$

and $g(r,t)$ is given by Eq (30).

When c_l and c_t are different, $\boldsymbol{f}$ and $\boldsymbol{g}$ are given by Eqs (38)-(41) or by (43)-(47), where the speed c is correspondingly replaced by c_l and c_t. In that case, the decoupling of the equations of motion as in Eq (27) ensures that the irrotational and solenoidal parts each propagate individually at their corresponding speeds, and their sum obeys Eq (32). At $t \to 0$, the boundary condition is obeyed since $g(r,t) \to g_0(r) = \frac{V}{\alpha} \delta\left(\frac{\boldsymbol{r}}{l}\right)$, and $\boldsymbol{f} \to \mathrm{irrot}(g_0 \hat{\boldsymbol{z}})$ and $\boldsymbol{g} \to \mathrm{solen}(g_0 \hat{\boldsymbol{z}})$. These analytical results were verified against the direct solution obtained from numerically solving Eq (32).

III. NUMERICAL RESULTS FOR POKING

To validate the preceding analysis, we carry out a series of molecular dynamics simulations of one- and three-dimensional solids – a linear chain and a face-centered-cubic (FCC) lattice respectively – interacting via a Lennard-Jones potential:

$$U^{(\mathrm{LJ})}(r) = 4\epsilon \left[\left(\frac{\sigma}{r}\right)^{12} - \left(\frac{\sigma}{r}\right)^{6} \right], \tag{48}$$

where the equilibrium separation between atoms was taken as $a = 0.5$ nm, the mass in atomic mass units as $m = 108$ amu, and the Lennard-Jones parameters as $\epsilon = 6.9 \cdot 10^{-20}$ J (0.431 eV) and $\sigma = a \cdot 2^{-1/6}$. The interaction range was limited to third-nearest neighbors. Periodic boundary conditions were used. Note that the desynchronization propagation is identical within one period in periodic and infinite systems up until the desynchronization wave reaches the lattice boundary. The equations of motion were integrated by the stochastic velocity Verlet scheme set forth in Melchionna [14, Eq 34], with care being taken to allow the system to thermalize prior to the perturbation applied at time $t = 0$. The temperature used was 50 K, and the iteration time step 1 fs.

A. Infinite one-dimensional chain

The infinite one-dimensional chain provides a simple first case for applying the theory of Section II. Expanding the Lennard-Jones force to harmonic order about the equilibrium $r = a = 2^{1/6}\sigma$ and considering only nearest-neighbor interactions gives the wave speed

$$c \approx \sqrt{r^2 \partial^2 U^{(LJ)}(r)/\partial^2 r/m}\,|_{2^{1/6}\sigma} \approx \sqrt{72\epsilon/m} \approx 5263\,\mathrm{m/s}. \tag{49}$$

With Langevin damping $\alpha = 1.0\ \mathrm{ps}^{-1}$, we subject a chain to a poke of strength $V = 10\ \mathrm{m\ s}^{-1}$ at $x = 0$, and simulate until $t = 100$ ps. Figure 1 depicts the simulated time evolution of the poked atom's displacement, in comparison with Eq (9), with a speed of sound given by Eq (49).

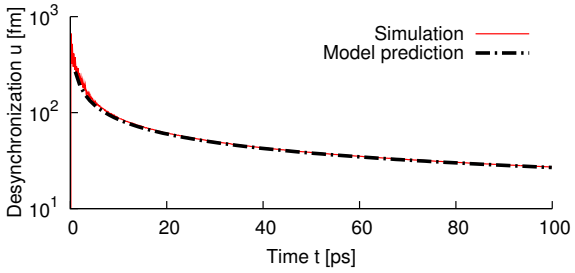

FIG. 1: (Color online) Simulated and theoretical desynchronization of the poked atom as a function of time for a one-dimensional chain of 1000 atoms (see Eq (9)).

Figure 2 shows a series of snapshots of the desynchronization of the atoms in the chain, beginning at 3 ps and 6 ps shortly after the poke as in Eq (7), through to the diffusive limit from Eq (9) at 20 ps. At small times a sharp front of the desynchronization propagates outwards from the poked atom as can be seen in Figs (a) and (b) for $t = 3$ ps and 6 ps, respectively. The atoms at $x > ct$ are completely synchronized. Soon after, the desynchronization around $x \lesssim ct$ becomes negligible and the sharp front is no longer observable. The

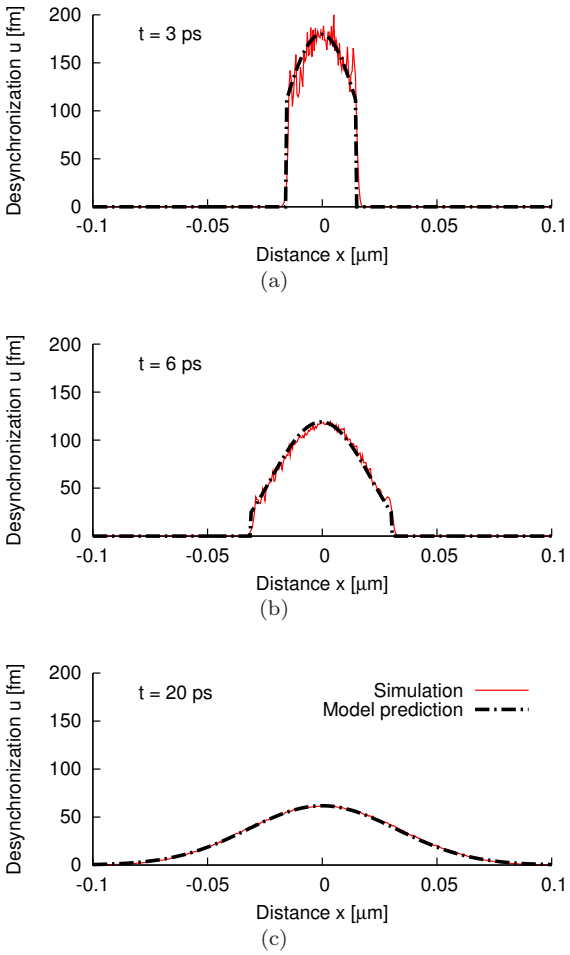

FIG. 2: (Color online) Propagation of the desynchronization wave in response to an instantaneous perturbation. The above three plots compare the analytic result of Eq (7) (Fig (a) - (b)) and Eq (9) (Fig (c)) with simulations of a one-dimensional Lennard-Jones chain. All parameters were taken from the theory.

Gaussian solution from Eq (9) becomes a very good approximation for all x once the diffusive limit has settled in (Fig(c)). The short wavelength oscillations in the simulation results at short times are due to high frequency underdamped modes whose behavior is not captured by the continuum solution as we explained in Section II B. The value of $\alpha = 1.0\ \mathrm{ps}^{-1}$ was chosen in these plots to ensure that friction is sufficiently large that the contribution from the underdamped modes is small. The desynchronization along these modes damps out quickly, as shown by the increasing smoothness of the simulation results as time proceeds.

B. Periodic one-dimensional chain

When the wave is allowed to reach the boundaries of the lattice, the behavior of the desynchronization corre-

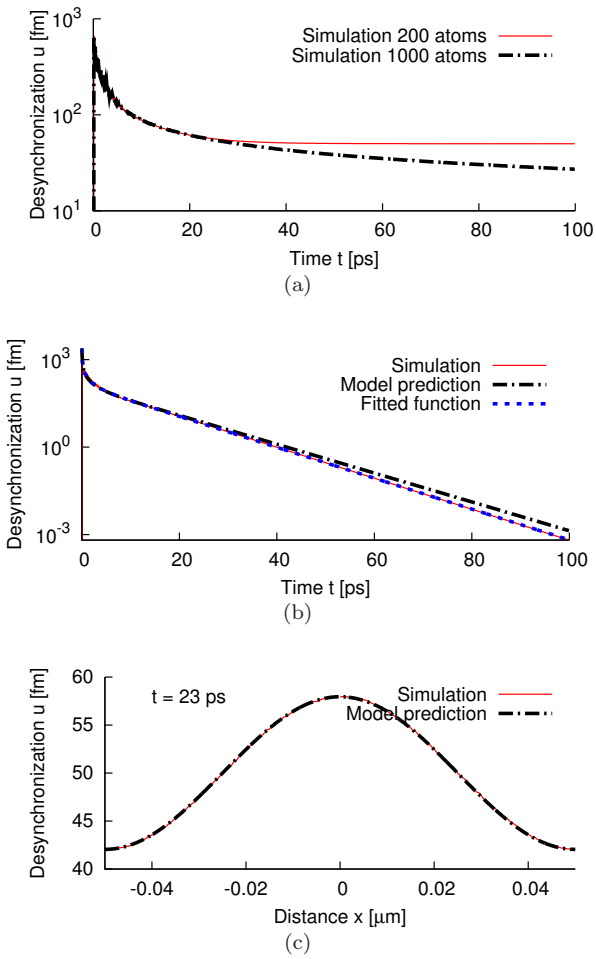

FIG. 3: (Color online) (a) Desynchronization of the poked atom for a one-dimensional chain of 200 atoms with periodic boundary conditions. Compare to Fig 1 for a chain of 1000 atoms. (b) Desynchronization of the poked atom after subtracting the displacement of the center of mass. The simulation is compared with the result of Eq (17) with and without fitting for the propagation speed. (c) Desynchronization of the chain at time $t = 23$ ps as compared with the theoretical result of Eq (19). In Figs (b) and (c) the propagation speed for the model prediction was obtained analytically from Eq (49).

sponds to the solution for periodic boundary conditions as in Eqs (17) and (19).

Figure 3(a) shows the desynchronization of the poked atom as a function of time for a one-dimensional chain of 200 atoms with periodic boundary conditions, friction coefficient $\alpha = 1.0\ \mathrm{ps}^{-1}$, and poking velocity $V = 10$ m/s without subtracting the displacement of the center of mass. On the same plot, the desynchronization of the poked atom for a chain of 1000 atoms from Fig 1 is also shown for comparison. It is clear that the desynchronization in the two cases is identical for short time, until the wave hits the boundaries of the lattice. At larger times the desynchronization of the poked atom decays as $1/\sqrt{t}$ for the chain of 1000 atoms, while for the chain of 200 atoms with periodic boundary conditions it reaches a constant asymptotic value given by $V/(\alpha N)$ (corresponding to the displacement of the center of mass).

Figure 3(b) shows the displacement of the same atom for the chain of 200 atoms after subtracting the center of mass displacement, with and without fitting for the propagation speed. Note the exponential decay at large times. In this plot the propagation speed c was fitted to the data and a value of $c \approx 5560$ m/s was obtained, which is larger by roughly 5% than the predicted value of $\sqrt{72\epsilon/m} \approx 5263$ m/s. The model prediction is also shown, for which all parameters were taken from the theory.

Figure 3(c) gives the desynchronization of the whole lattice for the same simulation as before, for time $t = 23$ ps, where all parameters were predicted analytically. Note the cosine dependence on the distance from the poked atom. These results clearly demonstrate that the desynchronization behavior is properly captured by the theory.

C. Three-dimensional lattice

In this section we are testing the theory from Eq (24) and (36) - (41) for an FCC cubic lattice of $30\times30\times30$ unit cells (108000 atoms), where we poke one atom in a certain direction and choose a coordinate system such that the z-axis is along the direction of poking. The poking velocity is set as $V = 10$ m/s and the friction coefficient as $\alpha = 100\ \mathrm{ps}^{-1}$. In three dimensions we observed that we need to simulate at a higher friction than in one dimension in order to use the analytical results we have derived in the continuum limit. To see how dimensionality comes into play, consider again Eq (18). In one dimension, the frequency of each mode was $\omega = ck$, for $k = \frac{2\pi}{L}n$, and we summed over $n \geq 1$. In three dimensions we have one wave number in each direction: $k_{x,y,z} = \frac{2\pi}{L}n_{x,y,z}$. When we sum over each mode, we now have a triple sum over n_x, n_y and n_z. Consequently, higher frequency modes now have a higher degeneracy than lower frequency ones, and the underdamped modes have a higher contribution than they did in the one-dimensional case. Therefore, in order to remain mainly in the overdamped regime and keep the effect of underdamped modes small, we need to increase the coupling constant α.

Figure 4 gives the desynchronization u_z of the poked atom as a function of time, where the theoretical prediction is given by

$$u_z(\boldsymbol{r} = 0, t) = \frac{l^3 V}{\alpha} \frac{2c_l^3 + c_t^3}{24\pi^{3/2}(c_l c_t)^3} \left(\frac{\alpha}{t}\right)^{3/2}. \qquad (50)$$

These results demonstrate that, for t larger than about 0.5 ps, the z component of the desynchronization for the poked atom decays as $t^{-3/2}$ (for an infinite lattice), as predicted by the model.

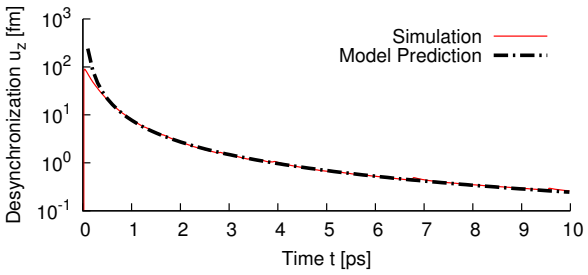

FIG. 4: (Color online) Simulated and theoretical desynchronization of the poked atom as a function of time for a cubic three-dimensional FCC lattice of 108000 atoms. The theoretical model predicts the desynchronization decreases as $t^{-3/2}$ at large times (see Eq (50)).The propagation speeds are given in Eq (51).

Figure 5 compares the desynchronization vector field obtained from the Langevin dynamics simulation with the analytic results from Section II C. The plots were obtained for time $t = 4$ ps and $t = 8$ ps and for $y = 0$ (the solution is invariant under rotations about the z-axis). The qualitative agreement between the simulations and the theory is very good.

In the three-dimensional case we fitted for the propagation speeds. Throughout the paper we use:

$$c_l^2 \approx \frac{70\epsilon}{m}$$
$$c_t^2 \approx \frac{18\epsilon}{m}. \qquad (51)$$

It should also be emphasized that the theory is based on the assumption that the solid is continuous and elastically isotropic. In the case of the Lennard-Jones solid, the speed of sound is not identical along different directions in the solid. Furthermore, the discrete nature of the system is more evident in 3D given that we can only afford to follow desynchronization across a few tens of lattice cells in each direction, as opposed to hundreds or thousands of atoms aligned in a chain in the one-dimensional case. This leads to deviations from the theoretical prediction which depend rather strongly on the orientation of the FCC lattice: our simulations produced somewhat different results depending on whether the poke was done in the direction of a nearest neighbor (e.g. $\langle 110 \rangle$), or in some other direction (e.g., $\langle 100 \rangle$ or $\langle 111 \rangle$) (note that we are still defining the coordinate system such that the direction of poking corresponds to the z-axis). To illustrate this effect, compare Fig 5 in which the direction of poking was $\langle 100 \rangle$ (towards a second-nearest neighbor), with Fig 6 where the atom was poked towards a nearest neighbor ($\langle 110 \rangle$). Apart from this difference, the parameters of the two simulations were identical, and in both cases we used the same speeds for the theoretical model. For instance it can be observed in Fig 5 that the simulation results are slightly lower that the prediction at $\theta = 0°$ ($x = y = 0$), while at the same angle in Fig 6 the simula-

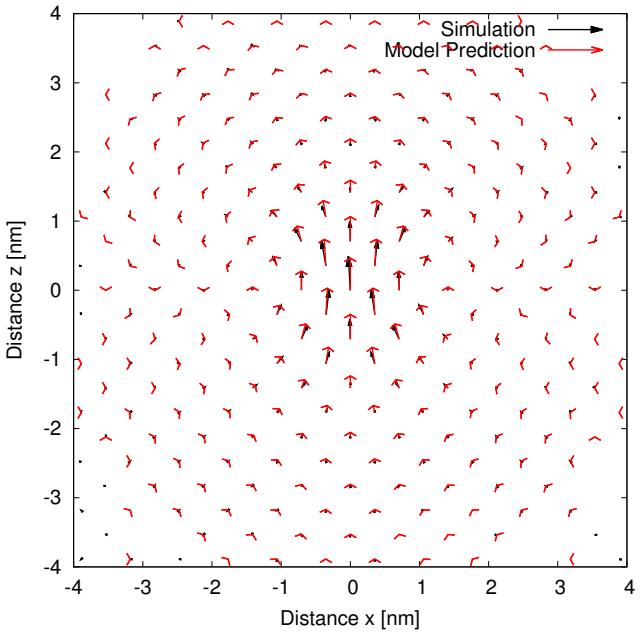

(a)

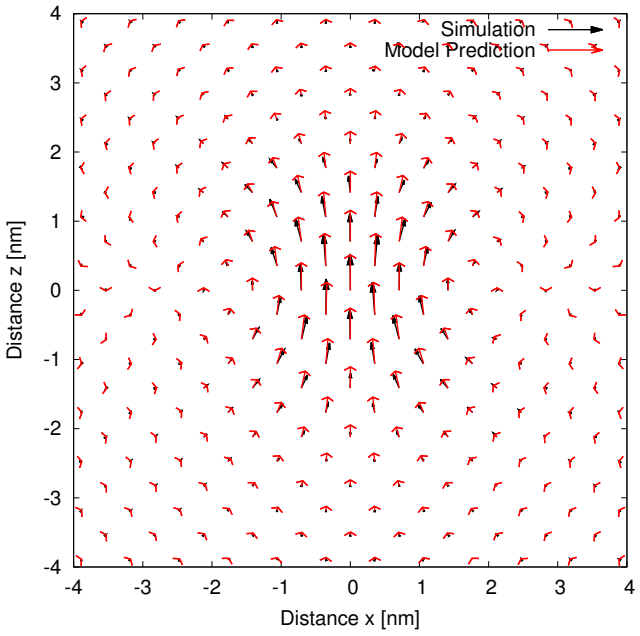

(b)

FIG. 5: (Color online) Desynchronization vector field $\boldsymbol{u}$ [fm] for $y = 0$ at $t = 4$ ps in (a) and $t = 8$ ps in (b). The arrows have been scaled by 0.48 at 4 ps and 1.5 at 8 ps for clarity. The Langevin dynamics simulation is compared to the analytic results of Section II C, where we have used the propagation speeds from Eq (51). In this simulation the poking was done in the direction of a second-nearest neighbor (i.e. $\langle 100 \rangle$ direction).

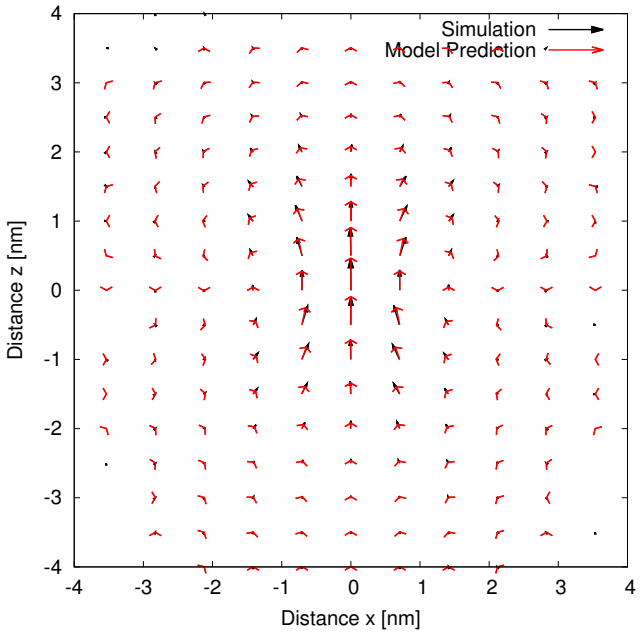

FIG. 6: (Color online) The same desynchronization vector field $\boldsymbol{u}$ [fm] as in Fig 5, but now the simulation was done by poking the atom towards a nearest neighbor (i.e. $\langle 110 \rangle$ direction). The propagation speeds for the model prediction are the same as in Fig 5, the time is $t = 4$ ps and the scaling 0.48 as in Fig 5 (a).

tion and prediction match very well. On the other hand, the simulation matches well at $\theta = \pm 45°$ in Fig 5, but is slightly larger in Fig 6.

Nevertheless, the analytical solutions still provide adequate estimates of the desynchronization, and enable the prediction of its spread throughout the lattice.

IV. PERSISTENT PERTURBATIONS: "SWITCHING"

We now turn our attention to temporally persistent disturbances applied to a system of atoms. This is achieved here through switching, i.e., the substitution of the sequence of random forces on a single atom in the system (the forces on the other atoms being otherwise matched). The desynchronization begins at the atom to which a different noise is applied and spreads with time. As will be shown in the next two sections, once the desynchronization wave hits an atom, it never fully recovers. In one dimension the desynchronization spreads through the chain and for each atom its variance continuously grows with time. In three dimensions, we show that the oscillations are spatially localized and decrease faster with distance from the switched atom. Interestingly, and contrary to the one-dimensional case, the desynchronization remains localized around the switched atom and does not propagate far through the medium.

A. Switching in one dimension

In the case of switching, we can obtain similar equations for the desynchronization as in the poking case, with the addition of an extra term:

$$\Delta A(x,t) = \xi(t)\delta(x/a) \tag{52}$$

giving the difference in the stochastic forces applied to the switched atom. We now find that the desynchronization evolves according to:

$$\frac{\partial^2 u}{\partial t^2} + \alpha \frac{\partial u}{\partial t} - c^2 \frac{\partial^2 u}{\partial x^2} = \frac{1}{m}\Delta A(x,t) \tag{53}$$

$$u(x,0) = 0 \tag{54}$$

$$\frac{\partial u}{\partial t}(x,0) = 0. \tag{55}$$

Here δ represents the Dirac-delta function as before, indicating that the difference in the stochastic forces applies only to the switched atom at $x = 0$. $\xi(t)$ is a Gaussian distributed random variable, where the expectation value and autocorrelation satisfy:

$$\langle \xi(t) \rangle = 0 \quad \text{and} \tag{56}$$

$$\begin{aligned} \langle \xi(t)\xi(t') \rangle &= 2 \cdot 2\alpha m k_B T \delta(t-t') \\ &= 2\Gamma\delta(t-t'). \end{aligned} \tag{57}$$

Note that this is twice the autocorrelation Γ of the random force, as the difference of two samples from a Gaussian distribution is also Gaussian-distributed, but with twice the variance. With respect to the initial conditions, the lattice at time $t = 0$ s does not change (initial velocities and positions are the same, even for the switched atom). Therefore, the difference in position and in velocity at $t = 0$ s is given by Eq (54) and (55).

In this case, Riemann's Method [8] gives the following solution for $u(x,t)$:

$$\begin{aligned} u\,(x,t) = &\frac{1}{2mc}\cdot \\ &\int_0^t \int_{x-c(t-t')}^{x+c(t-t')} I_0\left(\frac{\alpha}{2c}\sqrt{c^2(t-t')^2-(x-x')^2}\right) \\ &\cdot e^{-\frac{\alpha}{2}(t-t')}\Delta A(x',t')\mathrm{d}x'\mathrm{d}t' \end{aligned} \tag{58}$$

$$\begin{aligned} = &\frac{a}{2mc}\int_0^{t-\frac{|x|}{c}} I_0\left(\frac{\alpha}{2c}\sqrt{c^2(t-t')^2-x^2}\right) \\ &\cdot e^{-\frac{\alpha}{2}(t-t')}\xi(t')\mathrm{d}t', \end{aligned} \tag{59}$$

where t' is the time at which each force $\Delta A(x',t')$ is applied. Using Eq (59), we evaluate the variance $\langle u^2(x,t) \rangle$ over different random seeds by making use of the known

distribution of $\xi(t)$:

$$\langle u(x,t)\rangle = 0 \tag{60}$$

$$\langle u^2(x,t)\rangle = \frac{\Gamma a^2}{2m^2c^2} \int_0^{t-\frac{|x|}{c}} {I_0}^2\left(\frac{\alpha}{2c}\sqrt{c^2(t-t')^2-x^2}\right) \cdot e^{-\alpha(t-t')}\mathrm{d}t'. \tag{61}$$

Substituting for $\Gamma = 2\alpha m k_B T$, the prefactor shows that the rms desynchronization should be proportional to $\sqrt{T}$ where T represents the temperature.

A simpler analytical form can be obtained by using the asymptotic limit of the modified Bessel function I_0. The variance of the desynchronization becomes:

$$\langle u^2(x,t)\rangle = \frac{\Gamma a^2}{2\pi\alpha m^2c^2}\int_{\frac{|x|}{c}}^{t}\frac{1}{\delta t}e^{-\frac{\alpha x^2}{2c^2\delta t}}\mathrm{d}\left(\delta t\right) \tag{62}$$

where we define $\delta t = t - t\prime$ to be the time elapsed since the application of the random force. The approximation corresponds to the assumption that x (and consequently δt) is sufficiently large. In practice, we will see in Section V that when we compare to molecular dynamics simulations, this approximation is very good even for the nearest-neighbors of the switched atom.

Furthermore, if we take a Taylor expansion around $x = 0$ in Eq (62), we can see that for small fixed x (and any time t where the condition x^2/t is also negligible), the variance grows logarithmically in time:

$$\langle u^2(x,t)\rangle \approx \frac{\Gamma a^2}{2\pi\alpha m^2c^2}\left(\ln t - \ln\left(|x|/c\right)\right) \text{ for } \frac{\alpha x^2}{2c^2\delta t} \ll 1. \tag{63}$$

The switched atom itself is the only atom for which we cannot predict the magnitude of the desynchronization, since the predicted value goes to ∞ as $x \to 0$. In practice in a simulation this results in large, but still finite desynchronization for the switched atom.

Evaluating the integral in Eq (62), we obtain that the variance is given by:

$$\langle u^2(x,t)\rangle = \begin{cases} \dfrac{\Gamma a^2}{2\pi\alpha m^2c^2}\left(E_1\left(\dfrac{\alpha x^2}{2c^2t}\right) - E_1\left(\dfrac{\alpha\,|x|}{2c}\right)\right), \\ \qquad \text{for } |x| < ct \\ 0, \quad \text{otherwise,} \end{cases} \tag{64}$$

where $E_1(\xi) = \int_\xi^\infty \dfrac{e^{-\epsilon}}{\epsilon}d\epsilon$ is the exponential integral function.

Consequently, in one dimension the desynchronization spreads through the lattice and leads to a desynchronization amplitude that continuously grows with time.

B. Switching in three dimensions

We start again from the damped elastic wave equation as for poking, but with the additional noise term $\Delta\boldsymbol{A}(\boldsymbol{r},t) = \boldsymbol{\xi}(\boldsymbol{r},t)\,\delta\left(\dfrac{\boldsymbol{r}}{l}\right)$ which gives the difference in the applied forces on the switched atom (at $\boldsymbol{r} = 0$):

$$\ddot{\boldsymbol{u}} + \alpha\dot{\boldsymbol{u}} = \frac{1}{\rho}\left(\left(\lambda+\mu\right)\nabla\left(\nabla\cdot\boldsymbol{u}\right) + \mu\nabla^2\boldsymbol{u}\right) + \frac{1}{\rho}\Delta\boldsymbol{A}\left(\boldsymbol{r},t\right). \tag{65}$$

Here each component of $\boldsymbol{\xi}$ in cartesian coordinates is Gaussian distributed with the same variance 2Γ as in the one-dimensional case (c.f. Eq (57)). Therefore, the magnitude ξ of $\boldsymbol{\xi}$ has a Maxwell-Boltzmann distribution with the second moment given by $\langle\xi^2\rangle = 6\Gamma$. The direction of each $\Delta\boldsymbol{A}$ is randomly distributed with uniform probability.

As before, we expect that the desynchronization reaches a diffusion limit. The response to one single applied force difference $\Delta\boldsymbol{A}(t_0)$ at some time t_0 will therefore have the same time evolution as for poking. The overall solution will be given by the contribution of all applied forces $\Delta\boldsymbol{A}$ over time.

Consider first the solution for poking in an arbitrary direction $\hat{\boldsymbol{n}}$ defined by azimuthal angle ψ and polar angle χ:

$$\hat{\boldsymbol{n}} = \left(\cos(\chi)\sin(\psi),\ \sin(\chi)\sin(\psi),\ \cos(\psi)\right)^t. \tag{66}$$

The solution was described in Section II C (see Eqs (34)-(41)).

Now replace the poking velocity V by $1/m$ (with m the mass of the atoms), and denote the resulting solution by

$$\boldsymbol{u}_{\psi,\chi}(\boldsymbol{r},t) = \boldsymbol{f}_{\psi,\chi}(\boldsymbol{r},t) + \boldsymbol{h}_{\psi,\chi}(\boldsymbol{r},t) \tag{67}$$

with $\boldsymbol{f}$ and $\boldsymbol{h}$ the irrotational and solenoidal parts propagating at speeds c_l and c_t respectively.

Then the solution for switching in three dimensions is:

$$\boldsymbol{u}^{\text{switch}}(\boldsymbol{r},t) = \int_0^{t-\frac{r}{c}}\boldsymbol{u}_{\psi(t'),\chi(t')}(\boldsymbol{r},t-t')\xi(t')dt', \tag{68}$$

where $\psi(t')$, $\chi(t')$, and $\xi(t')$ are all independent random variables describing the force difference $\Delta\boldsymbol{A}$ applied at time t'. The equation above reflects the fact that it takes a minimum time r/c for a wave starting at the origin to reach an atom at distance r. The wave front for the r component $u_r(r,t)$ behaves as the wave front of a longitudinal wave since the desynchronization is in the direction of the wave propagation. Therefore the wave front propagates radially outwards with speed c_l. Similarly, the wave front for the θ and ϕ components $u_\theta(r,t)$ and $u_\phi(r,t)$ behave as the wave fronts of shear waves, and travel radially outwards with speed c_t. As a result, the speed c in the integration limit above should be replaced by c_l for u_r and by c_t for u_θ and u_ϕ.

As for switching in one dimension, we are interested in characterizing the expectation value and variance of the desynchronization, and their evolution in time. It is easy to show that the expectation value of the desynchronization is zero. This is expected since the system is spherically symmetric for uniformly distributed directions of the applied forces. What remains to be done is to compute the variance.

For two arbitrary independent random variables X and Y, the variance of their product is [15]:

$$\begin{aligned}\mathrm{Var}(XY) &= \langle X\rangle^2 \mathrm{Var}(Y) + \langle Y\rangle^2 \mathrm{Var}(X) + \mathrm{Var}(X)\mathrm{Var}(Y) \\ &= \left\langle X^2\right\rangle \mathrm{Var}(Y) + \langle Y\rangle^2 \mathrm{Var}(X). \end{aligned} \tag{69}$$

Now take X to be the magnitude $\xi(t)$ obeying $\langle\xi(t)\xi(t')\rangle = 6\Gamma\delta(t-t')$ as we've explained earlier, and Y to correspond to the angular part: $\hat{\boldsymbol{n}}\cdot\hat{\boldsymbol{r}}$, $\hat{\boldsymbol{n}}\cdot\hat{\boldsymbol{\theta}}$, or $\hat{\boldsymbol{n}}\cdot\hat{\boldsymbol{\phi}}$. For uniform distribution of the direction, the joint probability density function of ψ and χ is $\sin(\psi)/(4\pi)$, from where the expectation value and variance of the angular parts are:

$$\langle\hat{\boldsymbol{n}}\cdot\hat{\boldsymbol{r}}\rangle = 0 \tag{70}$$

$$\mathrm{Var}(\hat{\boldsymbol{n}}\cdot\hat{\boldsymbol{r}}) = \frac{1}{4\pi}\int_0^\pi d\psi \int_{-\pi}^{\pi} d\chi \sin(\psi)(\hat{\boldsymbol{n}}\cdot\hat{\boldsymbol{r}})^2 = \frac{1}{3}. \tag{71}$$

The same results are obtained for $\hat{\boldsymbol{n}}\cdot\hat{\boldsymbol{\theta}}$ and $\hat{\boldsymbol{n}}\cdot\hat{\boldsymbol{\phi}}$.

Putting everything together, the variance of the desynchronization for switching (written in spherical coordinates) is given by:

$$\mathrm{Var}(u_i^{\mathrm{switch}})(r,t) = 2\Gamma\int_{r/c}^{t} \mathrm{d}\delta t\, u_i(r,\delta t)^2, \tag{72}$$

where the index i stands for the radial and angular components $i = r,\ \theta,\ \phi$; $u_i = f_i + h_i$; and f_i and h_i are given by Eqs (38)-(41) (with V replaced by $1/m$, and c by c_l and c_t respectively). The propagation speed c in the integration limits corresponds to c_l for $u_r(r,t)$, and c_t for $u_\theta(r,t)$ and $u_\phi(r,t)$ respectively. As in the one-dimensional case, we have changed variables: $\delta t = t - t'$ represents the time elapsed since the application of the random force at time t'.

We were not able to analytically perform the above integral in terms of f_i and h_i. Instead, numerical integration is used to compute the variance of the desynchronization. The numerical integrations show that for any fixed r, the desynchronization reaches a finite asymptotic value.

To isolate the dependence on r, we note that $u_i(r,\delta t)$ can be written as $\delta t^{-3/2}\bar{u}_i(\delta t/r^2)$, where $\bar{u}_i(\delta t/r^2)$ is a function of $\delta t/r^2$. Changing variables $\tau \equiv \delta t/r^2$, we get:

$$\mathrm{Var}(u_i^{\mathrm{switch}})(r, t\to\infty) = \frac{2\Gamma}{r^4}\int_{1/rc}^{\infty} \mathrm{d}\tau\, \bar{u}_i(\tau)^2, \tag{73}$$

which goes roughly as $1/r^4$.

Therefore, we have seen that, contrary to the one-dimensional case, the desynchronization remains localized in three dimensions and does not diverge to infinity as $t\to\infty$. Instead, its rms decreases as $1/r^2$ with distance from the switched atom. In the next section we will compare our results with molecular dynamics simulations of three dimensional FCC crystals.

V. NUMERICAL RESULTS FOR SWITCHING

In this section we test our analytical results for persistent perturbations against molecular dynamics simulations. The desynchronization for each simulation is now dependent on the exact sequence of random noise forces applied on the switched atom, and we therefore average over many realizations to compute the rms desynchronization.

A. Switching in one dimension

We start with a one-dimensional chain of 3200 atoms interacting via the Lennard-Jones potential, with friction coefficient $\alpha = 1$ ps^{-1} and temperature 10 K. The simulation results are averages over 400 simulations initialized with different random seeds, while the theoretical prediction is given by the square root of the variance found in Eq (64). Note that the predicted rms at $x\to 0$ was infinite for the continuum approximation. In practice in a molecular dynamics simulation this results in finite but large oscillations of the switched atom over time.

Figure 7 shows the predicted and simulated rms desynchronization as a function of time for three different atoms: at $x = a = 0.5$ nm (namely the first neighbor of the switched atom), $x = 50$ nm, and $x = 200$ nm. As can be seen in Fig 7, the agreement between predictions and simulations is excellent, even at small times and distances. As x increases, the simulated rms desynchronization becomes smoother since the high frequency oscillations imposed on the switched atom as a result of applying the random noise sequence decay as they propagate further from the switched atom.

Figure 8 shows the predicted and simulated rms vs distance at times $t = 50$ ps, $t = 250$ ps and $t = 500$ ps, again according to Eq (64). It can be seen in the plots that the desynchronization continues to spread through the lattice with increasing time, leading to more and more atoms becoming desynchronized.

B. Switching in three dimensions

In three dimensions we tested the theory on an FCC lattice of $20\times 20\times 20$ cells (32000 atoms) with friction coefficient $\alpha = 100$ ps^{-1}. The simulated data was produced by averaging over 250 simulations. The theoretical prediction was obtained by numerically integrating

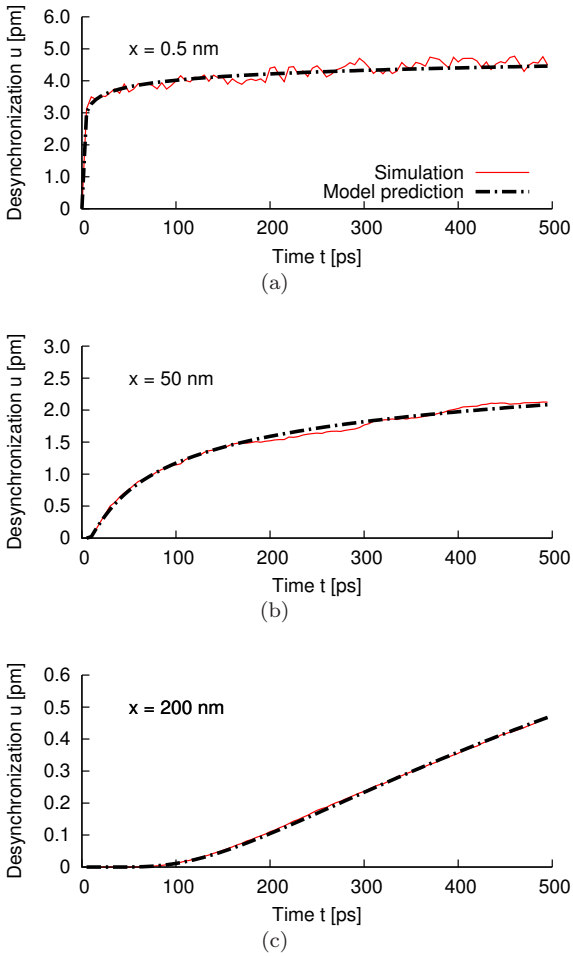

FIG. 7: (Color online) Root mean square of the desynchronization in one dimension for three different atoms as a function of time. The predicted value is given by the square root of Eq (64), while the simulation was obtained by taking the rms over 400 simulations.

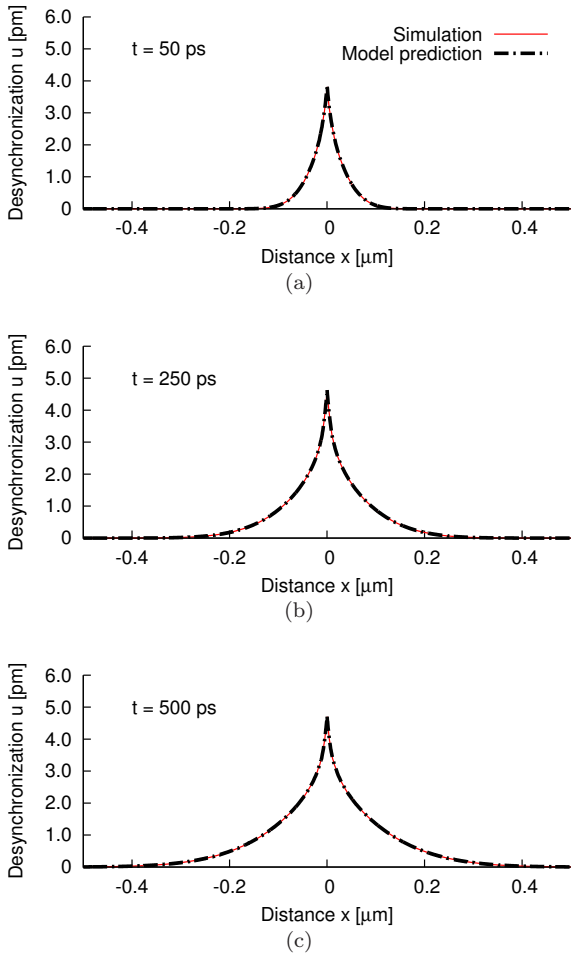

FIG. 8: (Color online) Predicted and simulated rms desynchronization for a one dimensional chain as a function of distance from disturbance, at three different times. The simulated data was obtained by taking the rms over 400 random seeds.

Eq (72), with the propagation speeds given in Eq (51). Once again, the predicted desynchronization at $r \to 0$ in the continuum limit is infinite, which in practice results in finite but high oscillations for the switched atom.

Figure 9 shows the radial component of the desynchronization of three different atoms vs time at $r = a$ (nearest neighbor of the switched atom), $r = a\sqrt{3}$, and $r = a\sqrt{12}$. As it can be seen in the figure, the desynchronization reaches a "steady state" with a constant rms. Atoms further away from the switched atom are hit by the desynchronization wave at later times, and reach the steady state at later times. Figure 10 shows the simulated and predicted rms of the desynchronization as a function of distance from the switched atom at times $t = 2.5$ ps, $t = 12.5$ ps and $t = 25$ ps. Note that indeed the disturbance stops growing in time and remains localized around the switched atom. The logarithmic plot at time $t = 25$ ps is shown in Fig 11. At $t \to \infty$ the rms desynchronization decreases with distance r from the switched atom roughly as $1/r^2$ as predicted. At large distances, since the desynchronization drops to very low values, the errors due to the anisotropy of the lattice become more visible, and appear as a highly regular pattern on the logarithmic plot. However, the prediction goes right through the simulated data and obeys the $1/r^2$ dependence.

VI. DISCUSSION AND CONCLUSIONS

Stochastic thermostats, such as the Langevin thermostat, are known to cause the synchronization of trajectories initialized at different points in phase space when the random noise is identical. Here, we quantified the spatiotemporal robustness of this effect. Our analysis builds on the response of one- and three-dimensional systems to an instantaneous perturbation (localized in time and space)

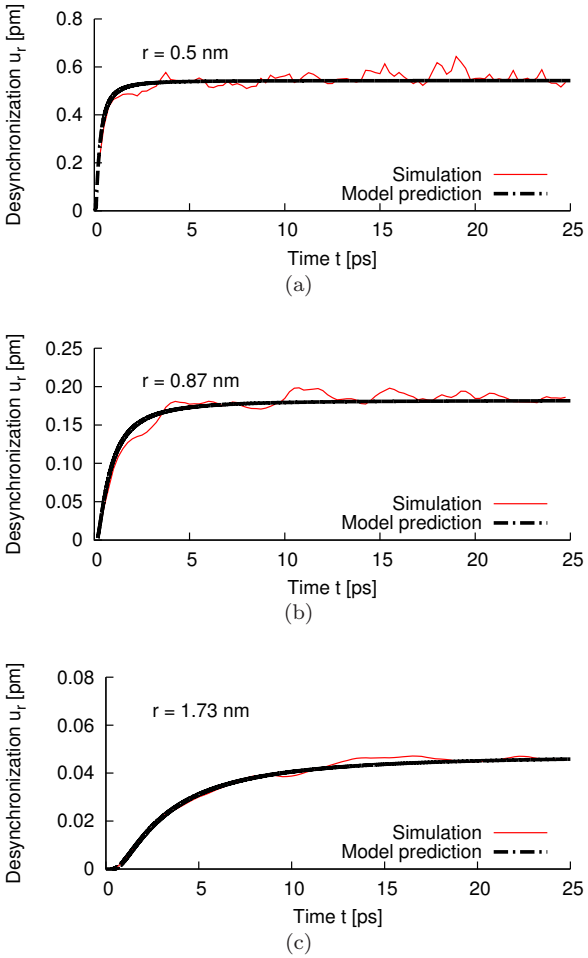

FIG. 9: (Color online) Rms of the radial desynchronization for an FCC lattice for three different atoms as a function of time, at $r = a$ (nearest neighbor of the switched atom), $r = a\sqrt{3}$, and $r = a\sqrt{12}$. The predicted value is given by the square root of Eq (72) (where the integral was evaluated numerically), while the simulation was obtained by taking the rms over 250 simulations.

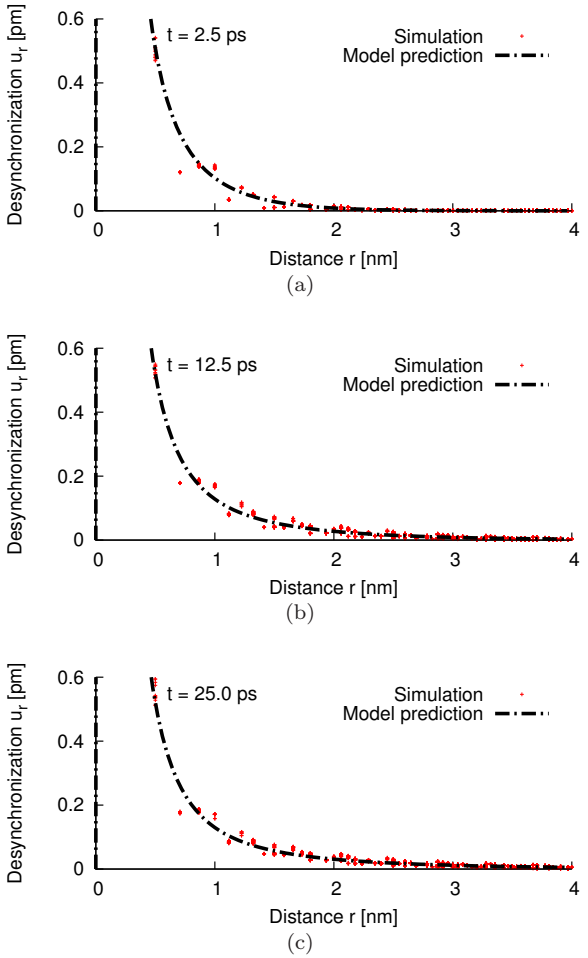

FIG. 10: (Color online) Predicted and simulated rms of the radial component of the desynchronization as a function of distance from disturbance, at three different times. The simulated data was obtained by taking the rms over 250 random seeds.

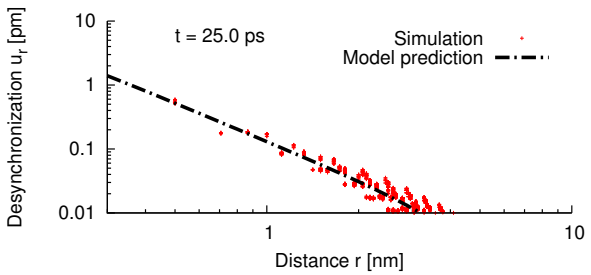

FIG. 11: (Color online) Logarithmic plot for the predicted and simulated rms of the radial component of the desynchronization at time $t = 25$ ps. At large time the desynchronization drops roughly as $1/r^2$ with distance from the switched atom.

in the case of Langevin molecular dynamics. Through the harmonic approximation of the Hamiltonian, we obtained the equation of motion for the evolution of the desynchronization in the continuum limit. The desynchronization was found to follow the damped wave equation in one dimension and the damped elastic wave equation in three dimensions. At long times the equations of motion become diffusive, and as a result the total desynchronization integrated over all space is conserved. Our analytical results, both in one and three dimensions, compare well to molecular dynamics simulations of crystals interacting via the Lennard-Jones potential in the high-coupling limit.

Building on these localized response functions, we extended our analysis to a time-persistent perturbation, in which we changed the entire random noise sequence for only one atom. In one dimension, the desynchronization is not localized, and its rms will continuously grow with time. Interestingly, however, this phenomenon is

not present in three-dimensional systems. Except for the switched atom, every other atom in the lattice reaches a "steady state", in which the variance of its desynchronization tends to a constant, asymptotic value. Furthermore, we found that at large time the rms drops roughly as $1/r^2$ with distance from the center of disturbance, i.e. desynchronization is spatially localized.

We note that the synchronization effect has been previously observed both in Langevin and Andersen thermostats, and also for rather complex systems (including bimolecules). Therefore, although our analysis has been focused on perfect crystals in the high coupling limit in order to keep the results analytical and rather simple, we expect that the localization behavior will be encountered in other more complex systems as well, and will be potentially useful in the development and understanding of advanced atomistic methods as discussed in the introduction.

Finally, it is worth pointing out that our results rely on a harmonic approximation of the potential energy landscape, which is more appropriate at low temperatures. In general, regions where the potential exhibits directions of negative curvature become increasingly thermally accessible as the temperature is increased, which locally leads to desynchronization. As discussed in Ref. 6, this can cause a decrease of the overall synchronization rate with increasing temperature. These observations should directly translate in the context of the present study, but we expect the broad features of the phenomena described here to be robust at typical solid-state temperatures.

Acknowledgments

The authors would like to acknowledge support from the National Science Foundation through grant DMS-0439872, and from Los Alamos National Laboratory. AG, SD, EJ and GC warmly thank Gang Lu at CSU Northridge and Mike Raugh and the staff at Institute for Pure and Applied Mathematics at UCLA for fruitful discussions and for the organization and running of the RIPS2009 program, which seeded this project. Work at Los Alamos National Laboratory (LANL) was supported by the United States Department of Energy (U.S. DOE), Office of Basic Energy Sciences, Materials Sciences and Engineering Division. LANL is operated by Los Alamos National Security, LLC, for the National Nuclear Security Administration of the U .S. DOE, under contract DE-AC52-O6NA25396.

Appendix: Solving the Elastic Diffusion Equation for Three-dimensional Poking

For equal propagation speeds $c \equiv c_l = c_t$, the elastic diffusion equation reduces to the diffusion equation with solution given by the three-dimensional Gaussian $\boldsymbol{u} = g(r,t)\hat{\boldsymbol{z}}$ from Eq (30). Since this is continuous, with continuous partial derivatives, and decays exponentially at infinity, we can decompose the desynchronization vector field into its irrotational and solenoidal parts $\boldsymbol{f}$ and $\boldsymbol{h}$ according to Helmholtz's theorem [12]. We compute the analytic forms of $\boldsymbol{f}$ and $\boldsymbol{g}$ by looking more closely into the derivation of Helmholtz's theorem. Using $\nabla^2 \frac{1}{|\boldsymbol{r}-\boldsymbol{r'}|} = -4\pi\delta(\boldsymbol{r}-\boldsymbol{r'})$, we write $\boldsymbol{u}$ as

$$\begin{aligned}\boldsymbol{u}(r,t) &= \int \mathrm{d}^3 r' \boldsymbol{u}(\boldsymbol{r'},t)\delta(\boldsymbol{r}-\boldsymbol{r'}) \\ &= -\frac{1}{4\pi}\nabla^2 \int \mathrm{d}^3 r' \boldsymbol{u}(\boldsymbol{r'},t)\frac{1}{|\boldsymbol{r}-\boldsymbol{r'}|}. \end{aligned} \tag{A.1}$$

Defining $\boldsymbol{G}(\boldsymbol{r},t) = \frac{1}{4\pi}\int \mathrm{d}^3 r' \boldsymbol{u}(\boldsymbol{r'},t)\frac{1}{|\boldsymbol{r}-\boldsymbol{r'}|}$, we obtain:

$$\boldsymbol{u}(\boldsymbol{r},t) = g(r,t)\hat{\boldsymbol{z}} = -\nabla^2 \boldsymbol{G}(\boldsymbol{r},t), \tag{A.2}$$

from where $\boldsymbol{G}(\boldsymbol{r},t) = G(r,t)\hat{\boldsymbol{z}}$ and $G(r,t)$ obeys the Poisson equation

$$g(r,t) = -\nabla^2 G(r,t). \tag{A.3}$$

Using that $g(r,t)$ is the three-dimensional Gaussian given by Eq (30), the solution to Poisson's equation is

$$\boldsymbol{G}(\boldsymbol{r},t) = G(r,t)\hat{\boldsymbol{z}} = \frac{l^3 V}{\alpha}\frac{1}{4\pi r}\mathrm{erf}\left(\frac{\sqrt{\alpha}r}{2\sqrt{t}c}\right)\hat{\boldsymbol{z}} \tag{A.4}$$

where erf is the error function. We write $\nabla^2\boldsymbol{G} = \nabla(\nabla\cdot\boldsymbol{G}) - \nabla\times(\nabla\times\boldsymbol{G})$, and identify

$$\boldsymbol{f}(\boldsymbol{r},t) = -\nabla(\nabla\cdot\boldsymbol{G}), \quad \boldsymbol{h}(\boldsymbol{r},t) = \nabla\times(\nabla\times\boldsymbol{G}). \tag{A.5}$$

The form of the solutions is nicer when written in spherical coordinates. Using $\boldsymbol{G} = G(r,t)\hat{\boldsymbol{z}}$, it can be shown that $\boldsymbol{f} = -(\hat{\boldsymbol{z}}\cdot\nabla)(\hat{\boldsymbol{r}}\frac{\partial G(r,t)}{\partial r})$, from where:

$$\boldsymbol{f}(\boldsymbol{r},t) = -\hat{\boldsymbol{r}}(\hat{\boldsymbol{z}}\cdot\hat{\boldsymbol{r}})\frac{\partial^2 G}{\partial r^2} - \hat{\boldsymbol{\theta}}(\hat{\boldsymbol{z}}\cdot\hat{\boldsymbol{\theta}})\frac{1}{r}\frac{\partial G}{\partial r} - \hat{\boldsymbol{\phi}}(\hat{\boldsymbol{z}}\cdot\hat{\boldsymbol{\phi}})\frac{1}{r}\frac{\partial G}{\partial r}. \tag{A.6}$$

The equation above can be generalized for a poke in some arbitrary direction $\hat{\boldsymbol{n}}$. In that case, we simply need to replace the unit vector $\hat{\boldsymbol{z}}$ in the equation above by the unit vector $\hat{\boldsymbol{n}}$. The solenoidal part is $\boldsymbol{h} = \hat{\boldsymbol{n}}g(r,t) - \boldsymbol{f}$ and has the same angular dependence as $\boldsymbol{f}$. We define:

$$\begin{aligned} f_r(r,t) &= -\frac{\partial^2 G}{\partial r^2}; & f_\theta(r,t) &= f_\phi(r,t) = -\frac{1}{r}\frac{\partial G}{\partial r} \\ h_r(r,t) &= (g + \frac{\partial^2 G}{\partial r^2}); & h_\theta(r,t) &= h_\theta(r,t) = (g + \frac{1}{r}\frac{\partial G}{\partial r}). \end{aligned} \tag{A.7}$$

The solutions are written in full in Eq (38)-(41). When the propagation speeds are different, one simply has to replace c by c_l or c_t in the final solutions for $\boldsymbol{f}$ and $\boldsymbol{g}$ respectively as described in Section II C.

[1] H. C. Andersen, J. Chem. Phys. **72** (1980).

[2] S. Chandrasekhar, Rev. Mod. Phys. **15**, 1 (1943).

[3] S. Fahy and D. R. Hamann, Phys. Rev. Lett. **69**, 761 (1992).

[4] A. Maritan and J. R. Banavar, Phys. Rev. Lett. **72**, 1451 (1994).

[5] M. Ciesla, S. P. Dias, L. Longa, and F. A. Oliveira, Phys. Rev. E **63**, 065202 (2001).

[6] B. Uberuaga, M. Anghel, and A. Voter, J. Chem. Phys. **120**, 6363 (2004).

[7] D. J. Sindhikara, S. Kim, and A. F. Voter, J. Chem. Theory Comput. **5**, 16241631 (2009).

[8] R. B. Guenther and J. W. Lee, *Partial Differential Equations of Mathematical Physics and Integral Equations* (Prentice-Hall, 1988), ISBN 0-13-651332-8.

[9] M. Abramowitz and I. Stegun, *Handbook of mathematical functions with formulas, graphs, and mathematical tables* (Dover publications, 1964).

[10] A. A. Maradudin, E. W. Montroll, G. H. Weiss, and I. P. Ipatova, *Theory of lattice dynamics in the harmonic approximation* (Academic Press, 1971).

[11] L. D. Landau and E. M. Lifshitz, *Theory of elasticity*, vol. 7 of *Course of Theoretical Physics* (Elsevier Ltd., 1986).

[12] D. J. Griffiths, *Introduction to Electrodynamics (3rd Edition)* (Benjamin Cummings, 1998), ISBN 9780138053260.

[13] G. B. Arfken and H. J. Weber, *Mathematical Methods for Physicists, Sixth Edition: A Comprehensive Guide* (Academic Press, 2005).

[14] S. Melchionna, J. Chem. Phys. **127**, 044108 (2007).

[15] L. A. Goodman, Journal of the American Statistical Association p. 708713 (1960).